FULL PAPER

ADVANCED FUNCTIONAL MATERIALS

Preparation of Homogeneously Dispersed Multiwalled Carbon Nanotube/Polystyrene Nanocomposites via Melt Extrusion Using Trialkyl Imidazolium Compatibilizer**

By *Séverine Bellayer*, *Jeffrey W. Gilman*,* *Naomi Eidelman*, *Serge Bourbigot*, *Xavier Flambard*, *Douglas M. Fox*, *Hugh C. De Long*, and *Paul C. Trulove*

Well-dispersed multiwalled carbon nanotube (MWNT)/polystyrene nanocomposites have been prepared via melt extrusion, using trialkylimidazolium tetrafluoroborate-compatibilized MWNTs. Quantification of the improvement is realized via transmission electron microscopy and laser scanning confocal microscopy image analysis. Differential scanning calorimetry and Fourier-transform infrared and X-ray diffraction analysis show evidence for a π-cation, nanotube–imidazolium interaction and the conversion from an interdigitated bilayer, for the imidazolium salt, to an ordered lamellar structure, for the imidazolium on the surface of the MWNTs.

1. Introduction

Carbon nanotubes (CNTs) were discovered in 1991, by Sumio Iijima.[1] The CNTs were prepared using a direct-current (DC) electric arc discharge (20 V, 100 A) in an inert atmosphere (He, Ar) at reduced pressure.[2] New techniques, such as catalytic carbon vapor deposition,[3] are now available to produce large quantities of CNTs. They can be single- or multiwalled. They may have diameters from 1 nm to 100 nm, and lengths from 0.1 μm to 100 μm. CNTs have demonstrated superior mechanical,[4] electrical,[5] and thermal[6] properties, and so have enabled new material applications.

The conductivity,[7] strength, toughness,[8] and flammability properties[9] of polymers may all be substantially improved by the addition of CNTs. However, the effective utilization of CNTs in nanocomposite applications may depend on the ability to homogeneously disperse them into the polymer matrix.[10] Furthermore, extensive interfacial interaction is required to achieve load transfer[11] across the CNT–polymer interface, to prevent re-aggregation during subsequent processing, and to enable other enhanced properties in the nanocomposite. Nanotubes preferentially aggregate into bundles, where adjacent tubes are held together by strong van der Waals' attractions.[12] Therefore, considerable research has been focused on CNTs to improve their compatibility with monomers and polymers.[13,14] Compatibilization can be achieved through functionalization, such as through covalently bonding organic groups directly to the CNTs.[13,15] Tour and co-workers reacted organic diazonium compounds with single-walled nanotubes (SWNTs) to facilitate incorporation into polystyrene (PS) by solution mixing in toluene;[16] Hill et al. functionalized SWNTs and multiwalled carbon nanotubes (MWNTs) with a PS copolymer, by esterification of carboxylic acid-functionalized nanotubes;[17] while Smith and co-workers reacted the carboxyl and hydroxyl groups on oxidized SWNTs with alkoxysilane-terminated amide acid polymers.[18] In some cases, covalent functionalization of the CNT sidewalls occurs to some extent. This process may disrupt the extended π-networks on CNT surfaces, diminishing both their mechanical and electronic properties. This is more of a concern for SWNTs, since MWNTs have interior tubes which would presumably remain intact. To avoid this potential effect, several groups have focused on finding non-covalent approaches to compatibilization. This can be accomplished through van der Waals' interactions between the alkyl chain of a surfactant and the aromatic surface of the CNT.[13,19] The non-covalent compatibilization may be a more facile and practical processing method. Two types of surfactants have been studied: non-ionic surfactants used with organic solvents for dispersion in epoxy resins,[14,20] and ionic surfactants, such

[*] Dr. J. W. Gilman, S. Bellayer, Dr. N. Eidelman[+]
National Institute of Standards and Technology
100 Bureau Drive, Gaithersburg, MD 20899-8665 (USA)
E-mail: jeffrey.gilman@nist.gov
Prof. S. Bourbigot
PERF of Ecole Nationale Supérieure de Chimie de Lille
BP108, 59652 Villeneuve d'Ascq Cedex (France)
Prof. X. Flambard
Laboratory ENSAIT-GEMTEX
9, rue de l'Ermitage—BP 30.329, 59056 Roubaix Cedex 01 (France)
Dr. D. M. Fox, Prof. P. C. Trulove
Chemistry Department, US Naval Academy
Annapolis, MD 21402 (USA)
Dr. H. C. De Long
Air Force Office of Scientific Research
Arlington, VA 22203 (USA)
[+] Second address: Paffenbarger Research Center, American Dental Association Foundation, 100 Bureau Drive - MS8546, NIST - Bldg. 224, Rm. A153, Gaithersburg, MD 20899-8546 USA.

[**] The authors thank the Air Force Office of Scientific Research (AFOSR-ISSA-01-0001) and the Federal Aviation Administration (DTFA 03-99-X-9009) for funding, and thank Dr. Kalman Migler for use of the mini-extruder and Dr. Li Piin Sung for use of the LSCM facilities.

  DOI: 10.1002/adfm.200400441

as sodium dodecyl sulfate (SDS), which can be used with water-soluble polymers. The latter has largely been investigated to disperse CNTs in water,[21–23] but it undergoes acid hydrolysis at 40 °C and has an onset temperature for decomposition of 190 °C; these properties limit its use for melt-blend processing, since most polymers are melt processed at 200 °C or above.

We have demonstrated that imidazolium salts are excellent cationic treatments for layered silicates (clays); they enable high-temperature curing and melt processing of polymer clay nanocomposites owing to their high thermal stability and excellent polymer compatibility when one of the imidazolium alkyl groups is a C16 aliphatic chain.[24] In addition, we have also been investigating the use of imidazolium-intercalated graphite to prepare polymer/graphite nanocomposites. Recently, Aida and co-workers reported that imidazolium salts can also interact with SWNTs[25] through "π-cation" interactions, which results in an ordering of the imidazolium salts into a layered crystalline phase.[26] The same group also utilized polymerization of an acrylate-functionalized imidazolium salt/SWNT mixture to prepare an ionomer/SWNT nanocomposite.

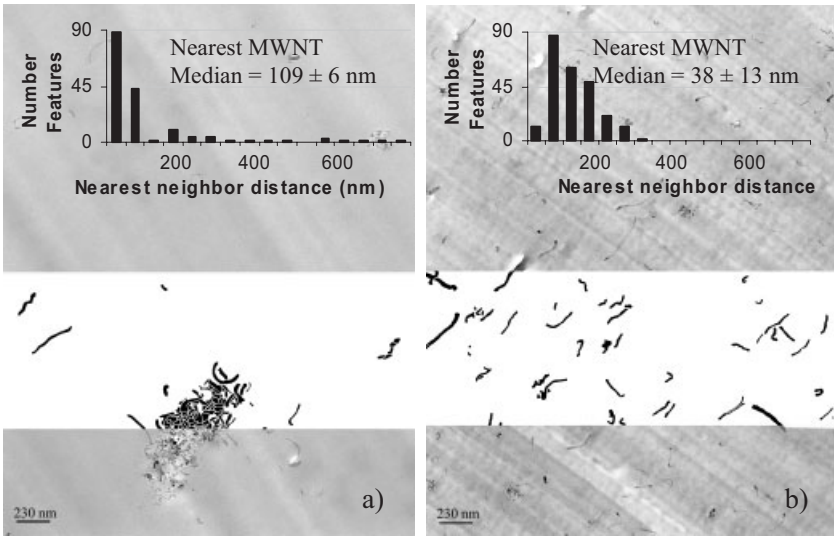

Figure 1. TEM images of PS/MWNT (without DMHDIm-TFB) (a) and PS/MWNT(1:1)DMHDIm-TFB (b).

In addition to the various methods that have to be developed to functionalize the CNTs, one needs to consider which processing method is best. Polymer/CNT nanocomposites can be prepared following three different methods: 1) via in-situ polymerization of monomer in the presence of the CNTs,[27] 2) from polymer solution, where both the polymer and the CNTs are dispersed in a solvent followed by evaporation,[28] and 3) from melt processing, which involves mechanical mixing of the molten polymer and the CNTs.[9] The latter, the melt-blending process, is commonly used in the polymer industry, and for this reason we are attempting to develop melt-processable, compatibilized CNTs for preparation of polymer/CNT nanocomposites.

2. Results and Discussion

A series of PS/MWNT blends were prepared using modified and unmodified MWNTs under a variety of processing conditions in a mini-twin-screw extruder (see Experimental). Melt blending of imidazolium-modified MWNTs and unmodified MWNTs with PS resulted in PS/MWNT nanocomposites with different MWNT dispersion. This is qualitatively apparent from the transmission electron microscopy (TEM) images of PS/MWNT (0.5 % mass fraction MWNTs), and PS/MWNT with the 1,2-dimethyl-3-hexadecylimidazolium tetrafluoroborate (DMHDIm-TFB): PS/MWNT(1:1)DMHDIm-TFB (0.5 % mass fraction MWNTs, and 0.5 % mass fraction DMHDIm-TFB) shown in Figure 1. In the TEM image of the simple PS/MWNT composite (Fig. 1a) very few single MWNTs can be observed; instead agglomerates (≈ 1 μm) of nanotubes dominate. In contrast, when DMHDIm-TFB-modified MWNTs are used, well-dispersed single nanotubes[29] can be observed in the TEM image (Fig. 1b). This is even easier to see in the enhanced images where the background has been removed (Figs. 1a,b). *Quantitative* characterization of nanocomposites is important for developing a detailed understanding of the methods used to prepare them. For this purpose, we have developed image-analysis techniques to characterize the TEM images. It is also important to perform quantitative image analyses on the TEM images to verify that the TEM data is representative of the entire sample.

We contend that, if the volume fraction of carbon nanotubes is much greater, or much lower, than the theoretical, the TEM is not representative of the entire sample in terms of additive concentration. Image analysis was done on PS/MWNT-untreated and PS/MWNT(1:1)DMHDIm-TFB composites. All image analysis was performed after removing the background on each image, as seen on Figure 1. The theoretical volume occupied by MWNTs in the nanocomposites is 0.27 vol.-% for 0.5 % mass fraction of MWNTs in PS. This is the approximate value obtained with image analysis for both samples (0.23 vol.-% was observed for the untreated sample and 0.35 vol.-% was observed for the modified sample). The main difference between the two samples appears when the dispersion measurement is performed. When MWNTs are untreated and directly incorporated in the PS, poor dispersion is obtained (median nearest-neighbor distance = 38 nm ± 13 nm). However, the use of DMHDIm-TFB greatly improves the dispersion of MWNTs in the PS matrix (median nearest-neighbor distance 109 nm ± 6 nm). The theoretical nearest-neighbor distance, for a perfectly mixed sample, is 120 nm ± 15 nm for the PS/MWNT-untreated and 132 nm ± 20 nm, for the PS/MWNT(1:1)DMHDIm-TFB sample. These results reflect the natural tendency of MWNT to agglomerate, as reported in the

literature,[13,30] and show that this behavior has been counteracted by the interaction with the imidazolium salt. It appears the DMHDIm-TFB acts as a compatibilizer, increasing the affinity of MWNTs for the PS, and preventing the natural tendency of MWNT to aggregate.

In terms of MWNT dispersion, the use of 1:4 and 1:19 MWNT-to-DMHDIm-TFB ratios produces a similar result to the 1:1-ratio sample; well-dispersed MWNTs are observed. However, holes appear in the TEM images (not shown) and a separate endotherm appears, at 70 °C, in the differential scanning aclorimetry (DSC) plot (Fig. 2) for the PS/MWNT(1:4)DMHDIm-TFB and PS/MWNT(1:19)DMHDIm-TFB samples.

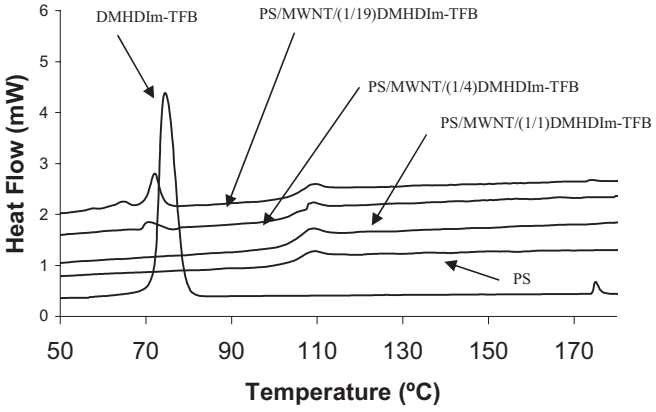

Figure 2. DSC curves of pure PS, PS/MWNT(1:1)DMHDIm-TFB, PS/MWNT(1:4)DMHDIm-TFB, PS/MWNT(1:19)DMHDIm-TFB, and DMHDIm-TFB at 10 °C min^{-1} under nitrogen flow.

Presumably, this is the characteristic melting peak of the excess imidazolium salt, which has phase separated from the PS matrix. The liquid-crystal clearing point, at 175 °C, is also seen in the DSC plot (Fig. 2) of the PS/MWNT(1:19)DMHDIm-TFB sample.[31] The DSC data (Fig. 2) for the sample with 1:1, DMHDIm-TFB-to-MWNT ratio does not show the characteristic melting peaks of the imidazolium salt.

This suggests that the imidazolium molecules may be at the MWNT–PS interface, either with an egde-on association of the imidazolium with the MWNTs, or a π-stacking-type interaction between the imidazolium and the MWNT surface (see Fig. 3). Studies of imidazolium-salt crystal packing has shown the preference for the π-stacking-type arrangement.[25] It has been seen in the literature that the PS glass-transition temperature (T_g = 108 °C) can increase a few degrees (less than 3 °C) with the addition of SWNTs.[32] Here, no significant effect was observed of imidazolium-treated MWNTs on the T_g of PS.

To evaluate the degree of mixing on the meso and micrometer scales, we imaged the PS/MWNT samples using a laser scanning confocal microscope (LSCM). This method requires the presence of a fluorescent dye, Nile blue A perchlorate (NB), in the polymer matrix. All samples were processed in the mini-twin-screw extruder at 20 rad s^{-1}, 195 °C, for either 1 min, or 10 min. All images (Figs. 4–6) have a corresponding intensity-versus-distance profile, taken from data along the horizontal center line shown in each image, which gives a quantitative indication of the level of variation in the image. The mean intensity ($\bar{x}$) and the relative noise ($2\sigma/\bar{x}$) have been calculated along this line; the lower the relative noise the more homogeneous is the sample. The false-color images are coded: green represents high-intensity fluorescence and blue represents low intensity. The low-intensity regions are assumed to be MWNT domains. The lower intensity in these regions is possibly resulting from a quenching mechanism in the vicinity of the MWNTs. Figures 4–6 are, respectively, those for PS + 0.5 % MWNTs (NB) processed for 1 min ($2\sigma/\bar{x}$ = 0.382), PS + 0.5 % MWNTs (NB) processed for 10 min ($2\sigma/\bar{x}$ = 0.184), and

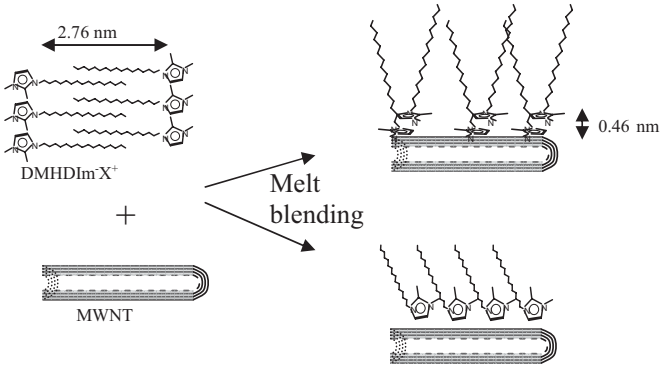

Figure 3. Interdigitated bilayer of $DMHDIm^-X^+$ (top left) melt blended with MWNTs to give π-stacking (top right), or end-on complexes (bottom right).

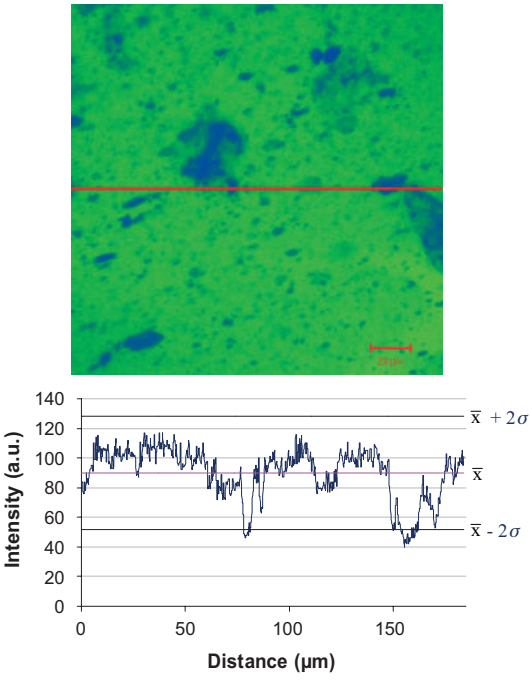

Figure 4. Composite confocal microscope image of PS + 0.5 % MWNT (NB) processed for 1 min and its corresponding intensity variation graph with a $2\sigma/\bar{x}$ = 0.382.

ADVANCED FUNCTIONAL MATERIALS

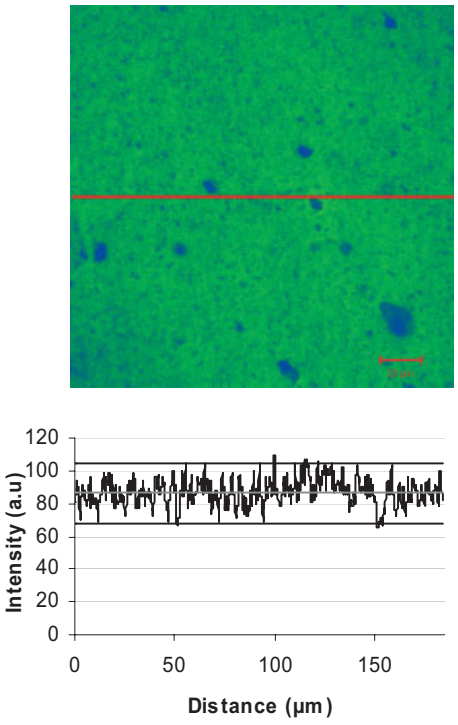

Figure 5. Composite confocal microscope image of PS + 0.5 % MWNT (NB) processed for 10 min and its corresponding intensity variation graph with a $2\sigma/\bar{x} = 0.184$.

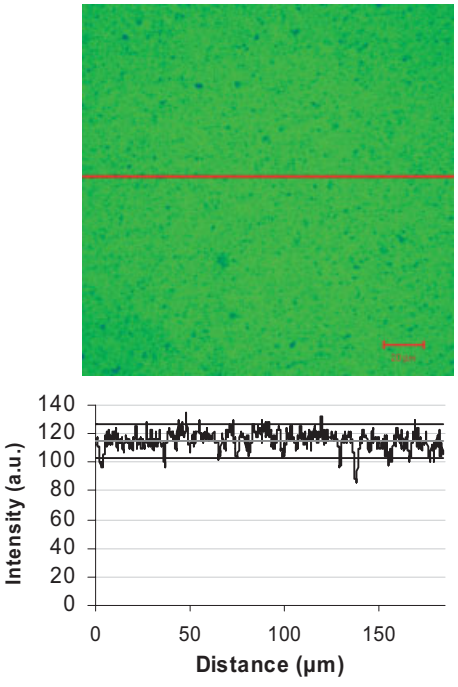

Figure 6. Composite confocal image of PS + 0.5 % MWNT + 0.5 % DMHDIm-TFB (NB) processed for 10 min and its corresponding intensity variation graph with a $2\sigma/\bar{x} = 0.096$.

PS + 0.5 % MWNTs + 0.5 % DMHDIm-TFB (NB) processed for 10 min ($2\sigma/\bar{x} = 0.096$). Figure 7 is from the MWNT-free control sample of PS with 0.5 % DMHDIm-TFB and NB, processed for 10 min; it indicates the "background" level of inhomogeneity of DMHDIm-TFB and NB in the PS ($2\sigma/\bar{x} = 0.089$).

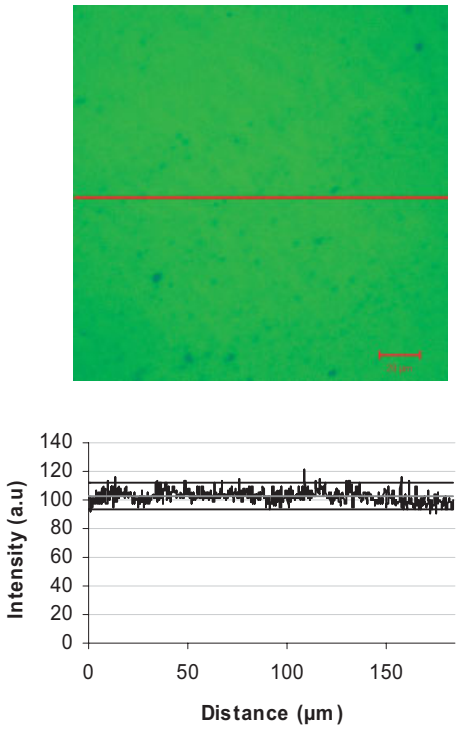

Figure 7. Composite confocal image of PS + 0.5 % DMHDIm-TFB (NB) processed for 10 min and its corresponding intensity variation graph with a $2\sigma/\bar{x} = 0.089$.

The first two samples (Figs. 4,5) reveal rather poor mixing (5 µm to 100 µm domains ($2\sigma/\bar{x} = 0.382$ and 0.184, respectively) of the MWNTs in the PS, in the absence of the imidazolium, even after 10 min residence time. However, the LSCM image from PS with 0.5 % MWNTs + 0.5 % DMHDIm-TFB (NB) (Fig. 6) provides clear evidence for the dispersing effect of the imidazolium on MWNTs in PS ($2\sigma/\bar{x} = 0.096$). Since the LSCM images are a composite of 150 images (200 nm thick focal plane, 150 slices or images) theses data provide a quantitative bulk-scale characterization method, and therefore are an excellent complement to the TEM data. Specifically, the Figure 5 LCSM image corresponds to the Figure 1a TEM image and the Figure 6 LCSM image corresponds to the Figure 1b TEM image. Therefore, on several length scales we have clear evidence of the compatibilizing effect of the imidazolium on MWNTs in PS.

To determine the nature of the interaction between imidazolium and MWNTs the IM/MWNT mixtures were characterized using X-ray diffraction (XRD) and Fourier-transform infrared

(FTIR) spectroscopy. Evidence for an interaction between DMHDIm-TFB and the MWNTs comes from XRD analysis shown in Figure 8. The XRD pattern of DMHDIm-TFB exhibits three reflections in the low angle region ($2\Theta = 3.2°$, 6.4°, 12.8°). These peaks are characteristic of the crystalline solid phase, and are most likely to be (00*l*) reflections from interdigitated-bilayer structure with an interlayer distance of 2.75 nm.[33] These three peaks tend to disappear when MWNTs are added to the DMHDIm-TFB, in particular for the 1:1 ratio. Additional peaks appear at higher angles are assigned to the alkyl-chain ordering.[33] This result is consistent with the fact that no separate phase is observed in the DSC plot (Fig. 2) for the PS/MWNT(1:1)DMHDIm-TFB blend. Furthermore, in separate experiments, the effect of the anion was evaluated; $DMHDIm^+ X^-$ salts ($X^- = PF_6^-$ and Cl^-) were melt blended with the MWNTs at 185 °C, and 170 °C, respectively. The hexafluorophosphate salt gave XRD results similar to the DMHDIm-TFB, i.e., loss of the bilayer peaks at high angles (data not shown). This indicates that, since the lamellar structure is observed independent of the anion associated with the $DMHDIm^+$, it must be the imidazolium cation that is interacting with the MWNT surface. Similar data was observed for the chloride salt; however, there was a small amount of residual bilayer observable in the XRD. This is due to the fact that $DMHDIm^+ Cl^-$ melt blending had to be done at 170 °C since it starts to decompose at 180 °C. This lower processing temperature, compared to the 185 °C used for all the other salts, is below the $DMHDIm^+ Cl^-$ clearing point and may have resulted in incomplete mixing and incomplete conversion of the $DMHDIm^+ Cl^-$ bilayer into the $DMHDIm^+ Cl^-$ MWNT complex.

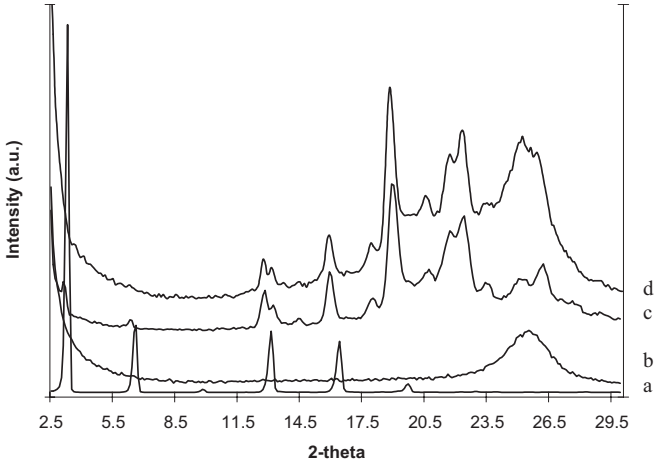

Figure 8. Powder X-ray diffraction pattern of a) DMHDIm-TFB, b) MWNTs, c) MWNT(1:4)DMHDIm-TFB, and d) MWNT(1:1)DMHDIm-TFB.

For each mixture, a peak appears in the higher angle region of the XRD spectra ($2\Theta = 19.1°$, $d = 0.46$ nm). This peak was identified in the literature as a π-stacking arrangement of the imidazolium cationic head.[25] Assuming a specific area of 0.1 μm^2 per MWNT and 3–4 imidazolium molecules per nm^2, a coverage calculation shows that even with the ratio 1:1 of DMHDIm-TFB/MWNTs, we have 3–4 times excess of imidazolium salt compared to the specific area of MWNTs. Thus, XRD spectra showed the conversion from an interdigitated-bilayer, liquid-crystal ($d = 2.8$ nm, melting point, m.p. 70 °C) for the imidazolium salt, to an ordered lamellar structure for the imidazolium on the surface of the MWNTs ($d = 0.46$ nm, no m.p.) in the 1:1 imidazolium-treated MWNTs.

To probe the interaction between the MWNTs and the imidazolium directly, we employed FTIR analysis. Figure 9 shows the IR curves of the pure DMHDIm-TFB and the MWNT-(1:1)DMHDIm-TFB samples. Two peaks at 3050 cm^{-1} and 3150 cm^{-1} in the DMHDIm-TFB spectra do not appear in the spectra of MWNT(1:1)DMHDIm-TFB. These two peaks are attributed to the CH···F hydrogen bonding between the $[BF_4]^-$ anion and the 4,5-hydrogens of the imidazolium ring.[34] The fact that these peaks disappear (or shift) in MWNT/(1:1)DMHDIm-TFB spectra provides strong evidence that an interaction exists between the imidazolium cation of the DMHDIm-TFB, and the MWNTs.[25] Sutto et al. have shown that a five membered imidazolium ring can lie nearly parallel to graphite sheets, and these FTIR results are consistent with their observation (see Fig. 3).[35] Presumably, this π-cation interaction perturbs the CH···F hydrogen bond normally present in the DMHDIm-TFB salt. Therefore, it is reasonable to assert that the DMHDIm-TFB is at the interface between the MWNTs and the PS matrix, and that it controls the dissolution of the MWNTs in the PS.

It is an important feature of this system that the imidazolium appears to be compatibilizing the MWNTs using the *reverse* of

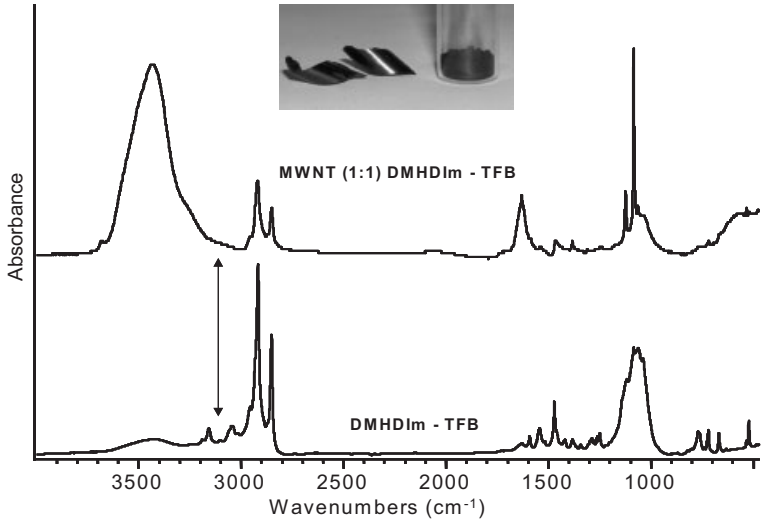

Figure 9. FTIR curves of MWNT(1:1)DMHDIm-TFB and DMHDIm-TFB, and a picture of MWNT(1:1)DMHDIm-TFB after cooling in the mini-extruder and after grinding.

the typical surfactant dispersion effect, e.g., where the alkyl chain of the surfactant interacts with the MWNT and the polar head group interacts with the water, or other polar media.[36] To our knowledge this is the first *direct* evidence of this type (π-cation) of interaction.

Thermogravimetric analysis (TGA) was performed on pure PS, PS/MWNT, and PS/MWNT(1:1)DMHDIm-TFB to evaluate their thermal stability. The mixing of untreated MWNTs or the DMHDIm without MWNTs into PS does not affect the thermal stability of PS; the onset and the maximum degradation temperatures are not changed compared to pure PS. Such behavior has been reported for several MWNT/polymer nanocomposites.[9,37] However, when DMHDIm-TFB-modified MWNTs are added, the onset and maximum degradation temperatures are increased by ≈ 20 °C ± 3 °C compared to pure PS (data not shown). This stabilization of the PS/MWNT(1:1)DMHDIm-TFB sample may be explained by the enhanced dispersion of MWNTs in the polymer matrix, which increases the contact surface between MWNTs and the polymer matrix, or by a better interfacial bonding between them. Further investigation of the percolation behavior and the mechanical properties of these nanocomposites are underway.

3. Conclusion

Using multiple characterization methods, we have demonstrated that trialkylimidazolium salt-compatibilized MWNTs may be used to prepare high-quality PS nanocomposites via melt extrusion. Evidence for a π-cation interaction between the nanotube and the imidazolium was found in the FTIR spectrum of the 1:1 imidazolium-treated MWNTs. Novel TEM-image analyses, and confocal microscopy of the PS(1:1)Im-MWNT nanocomposite, allowed quantitative evaluation of the superior dispersion of the imidazolium-treated MWNTs on length scales ranging from the nanometer to the millimeter. DSC revealed no phase-separated imidazolium, and TGA showed a 20 °C improvement in thermal stability. The further characterization of imidazolium-modified MWNTs in other polymers and applications is underway in our laboratories.

4. Experimental [38]

4.1. Materials

Purified multiwalled carbon nanotubes (MWNTs) were purchased from Seldon laboratories, LLC. Seldon specifies that the MWNTs are ≈ 98 %, pure, and with outer diameters 10 nm to 50 nm and lengths up to 2 μm. The imidazolium salts used include: 1,2-dimethyl-3-hexadecylimidazolium tetrafluoroborate, DMHDIM-TFB, and $DMHDIm^+ X^-$ salts ($X^- = PF_6^-$ and Cl^-). The imidazolium salts were synthesized according our published procedures [24]. DMHDIm-TFB has an onset of decomposition of 325 °C. The polystyrene (PS) used was STYRON 663 from Dow Chemical.

4.2. Processing

Three masterbatches of MWNTs modified with DMHDIm-TFB were prepared with different mass-fraction ratios of imidazolium to MWNTs, 1:1, 4:1, and 19:1. DMHDIm-TFB exhibits a liquid-crystalline transition (clearing point) at 175 °C. Therefore, DMHDIm-TFB and the MWNTs were melt mixed at 185 °C, in a conical co-rotation twin-screw mini-extruder (DACA) at 5.2 rad s^{-1} for 2 min. After cooling, MWNT/DMHDIm-TFB blends gave a solid material that was ground into a powder and was added to the PS during melt mixing. Three different MWNT/DMHDIm-TFB blends (MWNT content 0.5 % mass fraction) were melt mixed with PS at 195 °C at 26 rad s^{-1} for 5 min in the mini-extruder. Each sample used a different ratio of imidazolium to MWNT (1:1, 4:1, and 19:1) (respectively: PS/MWNT(1:1)DMHDIm-TFB, PS/MWNT(1:4)DMHDIm-TFB, and PS/MWNT(1:19)DMHDIm-TFB). A PS/MWNT reference with 0.5 % mass fraction MWNTs *without* any imidazolium treatment was prepared as above (PS/MWNT-untreated).

4.3. Characterization and Measurements

Powder X-ray Diffraction (XRD): XRD experiments were performed on a Bruker AXS D8 powder diffractometer. The *d*-spacing was calculated from peak positions using Cu Kα radiation ($\lambda = 0.15418$ nm) and Bragg's Law. Standard X-ray measurements of ground MWNT/DMHDIm-TFB were performed over a 2θ scanning range of 2.5° to 30°.

Transmission Electron Microscopy (TEM) Image Analysis: All samples were ultra-microtomed with a diamond knife on a Leica Ultracut UCT microtome at room temperature to give sections with a nominal thickness of 100 nm. The sections were transferred to Cu/Rh grids of 400 mesh. Bright-field TEM images of nanocomposites were obtained at 120 kV under low-dose conditions with a Philips 400T electron microscope. The materials were sampled by taking several images of various magnifications with two to three sections per grid to ensure that the analysis was representative of the sample. To quantify the dispersion of MWNTs in the PS with, or without, imidazolium treatment, image analysis was performed using four representative TEM pictures for each sample. Pictures used for image analysis are all TEM images taken at the exact same magnification, 22 000×, in order to distinguish individual MWNTs. Each of these images is separated by at least 100 μm. Schwarz and Exner [39] showed that a histogram of the distribution of the distances between nearest neighbors can characterize a distribution better than the location of individual features. Once the coordinates of the centroid points or mid-points representing each feature have been determined [40], the straight-line distance between the nearest neighbor for each points are calculated and used to construct the histogram. Actually, the distance between any pairs of neighbors, second nearest, etc., can be used instead, but in most cases the nearest-neighbor pairs are the easiest to identify. The nearest-neighbor distance of each point has been computed and the median calculated in the four images using Adobe Photoshop (version 6.0) and Fovea Pro (version 2.0) software. This value was compared to the theoretical distance obtained if the same number of features were randomly dispersed in the picture. This value was obtained using a Poisson random distribution

$$\bar{x} = \frac{0.5}{\sqrt{\frac{N}{\text{Area}}}} \quad (1)$$

where N is the number of features within the area of the field of view.

Laser Scanning Confocal Microscopy Analysis: A laser scanning confocal microscope (LSCM), model LSM510, from Carl Zeiss Inc. was used to image the samples. Four different polystyrene/MWNT/DMHDIm-TFB samples (4 g each) each containing the fluorescent

dye, Nile blue A perchlorate (NB, Aldrich) were processed in the DACA mini-extruder. Different parameters were varied, such as the residence time, the amount of MWNTs and DMHDIm-TFB. The composition and processing conditions are as follows :
– PS + 0.5 % MWNT (NB), 1 min, 20 rad s^{-1}, 195 °C
– PS + 0.5 % MWNT (NB), 10 min, 20 rad s^{-1}, 195 °C
– PS + 0.5 % MWNT + 0.5 DMHDIm-TFB (NB), 1 min, 20 rad s^{-1}, 195 °C
– PS + 0.5 % DMHDIm-TFB (NB), 1 min, 20 rad s^{-1}, 195 °C.

LSCM utilizes coherent laser light and collects light exclusively from a single plane (a pinhole sits conjugated to the focal plane) and rejects light out of the focal plane. A blue laser ($\lambda = 488$ nm) was used as the coherent light and images were taken at 50× magnification (scan size 184 μm × 184 μm), with a 1 airy unit pinhole. A British Petroleum (BP) 560 nm to 615 nm filter was necessary to recover exclusively the fluorescence of the dye after excitation by the laser. Several single images (optical slices) were taken by moving the focal plane and were combined by overlapping, to build up a two-dimensional intensity projection.

Thermogravimetric Analysis (TGA): TGA was performed on a Q500 TA instrument with platinum pans (10 mg samples), and a heating rate of 10 °C min^{-1} under nitrogen (flow rate 60 cm^3 min^{-1}). Differential scanning calorimetry (DSC) was recorded using a TA Instruments DSC2910. Data were collected during the second scan, using a scan rate of 10 °C min^{-1}, and a 50 cm^3 min^{-1} nitrogen flow rate (5 mg samples).

Fourier-Transform Infrared (FTIR) Analysis: MWNT(1:1)DMHDIm (0.84 mg) and DMHDIm (0.74 mg) were each thoroughly mixed with 400 mg of spectroscopic-grade KBr (dried) and pressed into transparent pellets (13 mm diameter, 1 mm thick). The IR spectra were measured between 4000 cm^{-1} and 400 cm^{-1} at a resolution of 2 cm^{-1} with 256 co-added scans using a Nicolet Nexus 670 FTIR spectrometer (Nicolet Instrument Corporation, Madison, WI) continuously purged with dry air.

Received: September 21, 2004
Final version: January 14, 2005

[1] S. Iijima, *Nature* **1991**, *354*, 56.
[2] P. M. Ajayan, *Condens. Matter News* **1995**, *4*, 9.
[3] R. Andrews, D. Jacques, D. Qian, T. Rantell, *Acc. Chem. Res.* **2002**, *35*, 1008.
[4] a) B. G. Demczyk, Y. M. Wang, J. Cumings, M. Hetman, W. Han, A. Zettl, R. O. Ritchie, *Mater. Sci. Eng. A* **2002**, *334*, 173. b) M.-F. Yu, O. Lourie, M. J. Dyer, K. Moloni, T. F. Kelly, R. S. Ruoff, *Science* **2000**, *287*, 637.
[5] C. A. Grimes, E. C. Dickey, C. Mungle, K. G. Ong, D. Qian, *J. Appl. Phys.* **2001**, *9*, 4134.
[6] S. Berber, Y.-K. Kwon, D. Tomank, *Phys. Rev. Lett.* **2000**, *84*, 4613.
[7] R. Andrews, D. Jacques, M. Minot, T. Rantell, *Macromol. Mater. Eng.* **2002**, *287*, 395.
[8] A. Dufresne, M. Paillet, J. L. Putaux, R. Canet, F. Carmona, P. Delhaes, S. Cui, *J. Mater. Sci.* **2002**, *37*, 3915.
[9] T. Kashiwagi, E. Grulke, J. Hilding, R. Harris, W. Awad, J. Douglas, *Macromol. Rapid Commun.* **2002**, *23*, 761.
[10] R. H. Baughman, A. A. Zakhidov, W. A. De Heer, *Science* **2002**, *297*, 787.
[11] L. S. Schadler, S. C. Giannaris, P. M. Ajayan, *Appl. Phys. Lett.* **1998**, *73*, 3842.
[12] A. Thess, R. Lee, P. Nikolaev, H. Dai, P. Petit, J. Robert, C. Xu, Y.-H. Lee, S.-G. Kim, A. G. Rinzler, D. T. Colbert, G. E. Scuseria, D. Tomanek, J. E. Fischer, R. E. Smalley, *Science* **1996**, *273*, 483.
[13] A. Hirsch, *Angew. Chem. Int. Ed.* **2002**, *41*, 11.
[14] S. Cui, R. Canet, A. Derre, M. Couzi, P. Delhaes, *Carbon* **2003**, *41*, 797.
[15] J. L. Bahr, J. M. Tour, *J. Mater. Chem.* **2002**, *12*, 1952.
[16] C. A. Mitchell, J. L. Bahr, S. Arepalli, J. M. Tour, R. Krishnamoorti, *Macromolecules* **2002**, *35*, 8825.
[17] D. E. Hill, Y. Lin, A. M. Rao, L. F. Allard, Y. P. Sun, *Macromolecules* **2002**, *35*, 9466.
[18] J. G. Smith, Jr., D. M. Delozier, J. W. Connell, K. A. Watson, *Polymer* **2004**, *45*, 133.
[19] A. Star, Y. Liu, K. Grant, L. Ridvan, J. Fraser-Stoddart, D. W. Steuerman, M. R. Diehl, A. Boukai, J. R. Heath, *Macromolecules* **2003**, *36*, 553.
[20] X. Gong, J. Liu, S. Baskaran, R. D. Voise, J. S. Young, *Chem. Mater.* **2000**, *12*, 1049.
[21] J. M. Bonard, T. Stora, J. P. Salvetat, F. Maier, T. Stockli, C. Duschl, L. Forro, W. A. de Heer, A. Chatelain, *Adv. Mater.* **1997**, *9*, 827.
[22] G. S. Duesberg, M. Burghard, J. Muster, G. Phillipp, S. Roth, *Chem. Commun.* **1998**, *3*, 435.
[23] V. C. Moore, M. S. Strano, E. H. Haroz, R. H. Hauge, R. E. Smalley, J. Schmidt, Y. Talmon, *Nano Lett.* **2003**, *3*, 1379.
[24] J. W. Gilman, W. H. Awad, R. D. Davis, J. Shields, R. H. Harris, Jr., C. Davis, A. B. Morgan, T. E. Sutto, J. Callahan, P. C. Trulove, H. De Long, *Chem. Mater.* **2002**, *14*, 3776.
[25] T. Fukushima, A. Kosaka, Y. Ishimura, T. Yamamoto, T. Takigawa, T. Aida, *Science* **2003**, *300*, 2072.
[26] J. C. Ma, D. A. Dougherty, *Chem. Rev.* **1997**, *97*, 1303.
[27] M. Cochet, W. K. Maser, A. M. Benito, M. A. Callejas, M. T. Martinez, J. M. Benoit, J. Schreiber, O. Chauvet, *Chem. Commun.* **2001**, 1450.
[28] B. Safadi, R. Andrews, E. A. Grulke, *J. Appl. Polym. Sci.* **2002**, *84*, 2660.
[29] In the TEM images the lengths of MWNTs appears smaller (10–500 nm) than the theoretical length (1–2 μm). Extrusion can cause some breakage of nanotubes [12] but here the main reason is the 100 nm thickness of the TEM section. Nanotubes are cut by the diamond knife during microtoming preventing observation of the real carbon-nanotube length.
[30] T. W. Odom, J.-L. Huang, P. Kim, C. M. Lieber, *J. Phys. Chem. B* **2000**, *104*, 2794.
[31] Since the TEM samples are microtomed at room temperature and the DMHDIm-TFB does not melt until 75 °C, the phase-separated DMHDIm-TFB domains may be pulling out of the sections. It is not likely that these holes are from degradation of the imidazolium salt; the DMHDIm-TFB used to modify the MWNTs has a high thermal stability (325 °C), much higher than the processing temperature (195 °C). Indeed, these holes do not appear in the TEM images of PS/MWNT-untreated sample, or for the sample with a 1:1 DMHDIm-TFB-to-MWNT ratio.
[32] J. Pham, C. Mitchell, J. Bahr, J. Tour, R. Krishanamoori, P. Green, *J. Polym. Sci. Part B: Polym. Phys.* **2003**, *41*, 3339.
[33] F. Neve, O. Francescangeli, A. Crispini, *Inorg. Chim. Acta* **2002**, *338*, 51.
[34] J. D. Holbrey, K. R. Seddon, *J. Chem. Soc., Dalton Trans.* **1999**, 2133.
[35] T. E. Sutto, P. C. Trulove, H. C. De Long, *Electrochem. Solid-State Lett.* **2003**, *6*, A50.
[36] O. Matarredona, H. Rhoads, Z. Li, J. H. Harwell, L. Balzano, D. E. Resasco, *J. Phys. Chem. B* **2003**, *107*, 13 357.
[37] S. Yang, J. R. Castilleja, E. V. Barrera, K. Lozano, *Polym. Degrad. Stab.* **2004**, *83*, 383.
[38] This work was carried out by the National Institute of Standards and Technology (NIST), an agency of the U. S. government and by statute is not subject to copyright in the United States. Certain commercial equipment, instruments, materials or companies are identified in this paper in order to adequately specify the experimental procedure. This in no way implies endorsement or recommendation by NIST. The policy of NIST is to use metric units of measurement in all its publications, and to provide statements of uncertainty for all original measurements. In this document, however, data from organizations outside NIST are shown, which may include measurements in non-metric units or measurements without uncertainty statements.
[39] H. Schwarz, H. E. Exner, *J. Microsc.* **1983**, *129*, 155.
[40] J. C. Russ, *The Image Processing Handbook*, 3rd ed., CRC Press LLC, Boca Raton, FL **1999**.

